

Sr–Al–Si co-segregated regions in eutectic Si phase of Sr-modified Al–10Si alloy

M. Timpel¹ N. Wanderka,¹ R. Schlesiger,² T. Yamamoto,³ D. Isheim,⁴ G. Schmitz,² S. Matsumura,³ and J. Banhart¹

¹ Helmholtz-Zentrum Berlin für Materialien und Energie, Hahn-Meitner-Platz 1, 14109 Berlin, Germany

² Institute of Materials Physics, Westfälische Wilhelms-Universität Münster, Wilhelm-Klemm-Str. 10, 48149 Münster, Germany

³ HVEM Laboratory, Kyushu University, Motooka 744, Nishi-ku, Fukuoka 819-0395, Japan

⁴ Department of Materials Science and Engineering, Northwestern University, 2220 Campus Drive, Evanston, IL 60208-3108, USA

*Correspondence should be addressed to: melanie.timpel@helmholtz-berlin.de; Tel.: +49 30 8062 42330; Fax: +49 30 8062 43059

Keywords: eutectic modification, Al-Si alloys, Atom Probe Tomography, Transmission Electron Microscopy

The addition of 200 ppm strontium to an Al– 10 wt.% Si casting alloy changes the morphology of the eutectic silicon phase from coarse plate-like to fine fibrous networks. In order to clarify this modification mechanism the location of Sr within the eutectic Si phase has been investigated by a combination of high-resolution methods. Whereas three-dimensional atom probe tomography allows us to visualize the distribution of Sr on the atomic scale and to analyse its local enrichment, transmission electron microscopy yields information about the crystallographic nature of segregated regions. Segregations with two kinds of morphologies were found at the intersections of Si twin traces: Sr–Al–Si co-segregations of rod-like morphology and Al-rich regions of spherical morphology. Both are responsible for the formation of a high density of multiple twins and promote the anisotropic growth of the eutectic Si phase in specific crystallographic directions during solidification. The experimental findings are related to the previously postulated mechanism of "impurity induced twinning".

1. Introduction

Minor additions of a few 100 ppm of certain specific modifying elements such as Sr, Na, Ca, Ba or Eu change the eutectic microstructure of Al-Si casting alloys drastically. The modification of the eutectic Si phase in an Al-Si alloy by Na was first reported in 1921 [1]. Since then, the modification effect has been the subject of many hundreds of publications and many reviews [2-4]. Several mechanisms of eutectic modification have been predicted. The two most established growth models of eutectic modification from coarse plate-like into fine fibrous Si morphology are, i) restricted growth of the "twin plane re-entrant edge" (TPRE) mechanism [5] based on {111} twinning and involving $\langle 112 \rangle$ directions [6, 7] and, ii), "impurity induced twinning" that can be explained by the adsorption of impurity atoms on {111} close packed planes, which promotes {111} twinning by displacing a {111} monolayer growth step to an alternative stacking sequence [8].

The formation of a high density of twins in Sr-modified Si fibres suggests that modifiers play an important role for Si twinning. A direct visualization of the modifying elements using conventional analytical methods is difficult because of the resolution limit of most imaging techniques and the very low amounts involved, e.g. just 80–120 ppm Sr in Al-Si alloys. Recently, X-ray fluorescence microscopy (μ -XRF) revealed that Sr segregates exclusively to the eutectic Si phase in an alloy Al– 10 wt.% Si– 1 wt.% Cu modified by 250 ppm Sr and is distributed homogeneously within the eutectic Si phase [9]. In contrast to this result, the investigation of the eutectic Si phase by means of atom probe tomography (APT) indicated a heterogeneous distribution of Sr [10]. Two distinct types of complex Sr–Al–Si co-segregations were identified. Type I co-segregations are of rod-like morphology and are located at the intersections of twin traces. They are responsible for the formation of multiple twins in the eutectic Si fibres and enable their growth in different crystallographic directions. Type II co-segregations are more extended than type I and are located close to the eutectic Al/Si interface. They restrict growth of the eutectic Si fibres and control their branching [10]. Both types contain Al, which was unexpected, since the solubility of Al in Si is negligible according to the binary phase diagram. In addition, no hint of the presence of Al in the eutectic Si phase has been reported up to now in the literature. Therefore, the distribution of Al within these segregated regions and its crystallographic location are of interest.

The objective of the present work was to further investigate in detail segregations within the Sr-modified eutectic Si fibres in an Al– 10 wt.% Si alloy using two complementary high-resolution methods, namely APT and high-resolution transmission electron microscopy (HRTEM). Both were employed to study the composition as well as crystallographic structure of nm-sized Sr- and Al-containing segregations.

2. Experimental

The preparation of Sr-modified Al – 10 wt.% Si alloy castings is described in detail in Ref. 10. After addition of the modifier Sr, the melt was cast into cylindrical rods ($\varnothing = 30$ mm, length = 200 mm). The chemical composition (in wt.%) of the as-cast alloy was determined by an optical emission spectrometer and is given in Table 1.

For atom probe analysis, the castings were sectioned perpendicular to the rod axes, cut into pieces of $5 \times 5 \times 1$ mm³ and mechanically polished. The polished surface was investigated via Scanning Electron Microscopy (SEM) in order to find areas of well-modified Al-Si eutectic (see Fig. 1(a)) suitable for the Focused Ion Beam (FIB)-based *in-situ liftout* technique [11,12]. A cross-sectional blank ($\sim 2 \times 10 \times 5$ μ m³ in size) was lifted out and positioned on a Mo substrate, see Fig. 1(b). In order to prepare thin needles suitable for APT analysis containing the required microstructural features such as Al/Si eutectic interfaces, the final specimen sharpening was performed using FIB annular milling patterns in a Zeiss 1540EsB CrossBeam[®] workstation. A defined sample rotation and SEM imaging were used to identify the location of Si fibres to be analysed by atom probe and to keep track of specific Al/Si eutectic interfaces during the FIB milling steps. Tip sharpening was stopped after a Si fibre and/or eutectic Al/Si interface appeared at the apex of the specimen with a final radius of curvature below 50 nm, see Fig. 1 (c). A laser-pulsed atom probe built at the University of Münster [13] was employed. Laser-pulsed atom probe analyses were performed with femtosecond pulses from a UV laser (wavelength $\lambda = 343$ nm) at 10^{-8} Pa pressure and ~ 55 K temperature with a pulse repetition rate of 200 kHz. A pulse

energy of 150 nJ was used for samples containing only eutectic Si phase at the apex of the needle.

The structural and chemical analysis of the eutectic Si fibres was carried out using a C_s -corrected JEOL JEM ARM200F transmission electron microscope operated at 200 kV and equipped with a newly developed energy-dispersive X-ray spectroscopy (EDX) system based on a Si drift detector with a sensing area of $\sim 100 \text{ mm}^2$.

3. Results and Discussion

Fig. 1(a) shows the eutectic microstructure of an Al– 10 wt.% Si alloy that has been fully modified by the addition of 200 ppm Sr. The eutectic Si phase (dark contrast) appears spherical in two dimensions, but in three dimensions it forms interconnected fibres as can be demonstrated by FIB tomography [14-16].

In order to analyse regions enriched in Sr and Al within such eutectic Si fibres and to get crystallographic information HRTEM was used. Fig. 2(a) illustrates regions of high twin density in a eutectic Si fibre imaged using BF STEM in an $\langle 110 \rangle$ orientation. Two of four possible $\{111\}$ twin traces are visible. Areas with dark contrast (corresponding to atoms with higher atomic number Z) are located mainly at the intersections of the twin traces. However, some of those dark areas seem to be distributed randomly. We assume that such randomly distributed areas with dark contrast are located at the intersections of the other $\{111\}$ twins not visible in this specific $\langle 110 \rangle$ orientation. The area marked by a square in Fig. 2(a) is shown in the HRTEM micrograph in (b), where disrupted crystal lattice planes are marked by circles. Such disrupted planes extend only over a distance of a few lattice constants and their size ranges here from 1 to 2 nm.

Such regions of high twin density within eutectic Si fibres have been investigated in detail using APT. Figure 3 displays a mass spectrum obtained from a eutectic Si fibre applying the evaporation conditions mentioned above (number of detected atoms $\sim 2 \times 10^7$). The laser-pulsed field evaporation produces singly and doubly charged Si and Al ions, whereas Sr is observed only in the doubly charged state. The mass spectrum exhibits additional $(\text{SiOH}_x)^+$ peaks at 45, 46, 47 amu and $(\text{SiOH}_x)^{2+}$ at 22.5, 23, 23.5 amu indicating the formation of silicon complex ions. This evaporation behaviour at short laser wavelength and high intensities is in good agreement with previous experimental observations for Si [17]. Since the presence of complex ions $(\text{SiOH}_x)^{y+}$ is a specific experimental evaporation effect of Si, the $(\text{OH}_x)^{y+}$ ions are not taken into account for further analysis. Signals with low intensities ($\sim 0.049 \pm 0.001 \text{ at.}\%$) in the mass range 35–37 amu with a distance of 0.5 amu could not unambiguously be attributed to any element or molecule. Details of the mass spectrum for doubly charged Sr ions are shown in the mass/charge interval 41–51 amu in Fig. 3(b). The major peak of Sr at 44 amu is well defined and the abundance ratio of the two peaks at 43 and 43.5 amu is very close to the natural abundance ratio. The presence of strong peaks for singly charged Ga ions are due to Ga implantation during specimen preparation by FIB milling and are ignored. Peaks corresponding to B^+ , P^+ , Ca^+ and signals in the mass range 35–37 amu are not considered for further analysis due to their homogenous distribution in the investigated volume.

Figure 4(a) shows a three-dimensional Sr map within the eutectic Si fibre as obtained by APT measurement. The analysed volume is about $39 \times 38 \times 290 \text{ nm}^3$ large and contains about 12×10^6 atoms. In this volume, two different enriched regions with Sr concentrations $> 0.6 \text{ at.}\%$ (red) and Al concentrations $> 5.0 \text{ at.}\%$ (blue) have been

identified and are shown as iso-concentration surfaces. Sr-rich regions already identified as Sr–Al–Si co-segregations of type I in a previous paper [10] appear as rods in 3D, whereas additional Al-rich regions have approximately spherical shape. The latter kind of Al-rich regions has not been described in Ref. 10. A small volume of $30 \times 30 \times 50 \text{ nm}^3$ with a few Sr-rich and Al-rich regions has been selected and is shown in Fig. 4(b). The chemical composition of both kinds of enrichments is calculated using the proximity histogram (proxigram) method [18].

The proxigram concentration profiles for Sr-rich regions are shown in Fig. 4(c). A representative concentration of the Sr-rich regions was obtained by averaging over the interior region 1.0–1.75 nm from the iso-surface. The chemical composition of rod-like Sr–Al–Si co-segregations varied from 2.6–2.8 at.% Sr, 6.2–11 at.% Al and 86.4–91 at.% Si. The amount of Sr in Sr–Al–Si co-segregations is almost constantly ~ 2.7 at.%, whereas the amount of Al varies and is 2–4 times higher than that of Sr. APT results reported previously [10] proved that Sr is exclusively located in the eutectic Si phase. This is inconsistent with our recently published results where Sr was found to be segregated to the eutectic Al/Si interface of a Sr-modified Al–15 wt.% Si alloy [19]. The explanation for this finding is that the APT experiments in Ref. 19 were carried out using voltage-pulsed field evaporation. Since Si is a semiconducting material it was not possible to detect Si from the eutectic Si phase. In contrast, Sr within the eutectic Si phase was detected and, therefore, all Sr atoms during field evaporation were collected and reconstructed artificially as a layer at the eutectic Al/Si interface [19]. Examples of the proxigram concentration profiles of the additional Al-rich regions with spherical morphology are shown in Fig. 4(d). The main components are Al and Si and the amount of Al at the centre of the Al-rich regions varied from 35–65 at.%. Sr is also present within the co-segregated regions but with a very small amount of ≤ 0.5 at.%. No other impurity elements were found within these regions. The diameter of Al-rich regions varied from 2–6 nm.

Figure 5(a) shows a bright-field scanning TEM (BF STEM) micrograph of regions with high twin density in a eutectic Si fibre oriented in $\langle 110 \rangle$ direction. Similar to Fig. 2, several $\{111\}$ twin traces are visible. However, here the $\langle 110 \rangle$ orientation is perpendicular to the Si twin intersections imaged. The same area in Fig. 5(a) has been obtained by high-angle annular dark-field (HAADF) STEM, see Fig. 5(b). The dark line in the marked square in Fig. 5(a) imaged by BF STEM appears in inverted contrast by HAADF STEM, see Fig. 5(b). Bright contrast in HAADF STEM corresponds to higher Z (atomic number) since the HAADF signal scales with Z^2 . Figure 5(c) shows the microstructure in higher magnification within the area marked by squares in Fig. 5(a) and (b). The crystal lattice and a bright linear feature marked by arrows are clearly visible. The width of the bright lines is only 1–2 interplanar spacings of $\{111\}_{\text{Si}}$ planes, whereas their length is here about 8 nm. Figure 5(d) shows an EDX mapping for Sr (red) and for Al (blue). An increased intensity of both elements compared to surrounding areas at the same locations where HAADF STEM detected Z contrast provides direct evidence that Sr and Al are segregated there. It can be concluded that the rod-like Sr–Al–Si co-segregations shown in Fig. 5(a) and (b) are located along the $\{111\}_{\text{Si}}$ trace in the image plane.

Correspondingly, Al-rich regions were also analysed by HRTEM. The results of BF STEM analysis are shown in Fig. 6(a). A two-dimensional lattice image of the eutectic Si fibre was taken with the incident beam parallel to one $\langle 110 \rangle$ direction. A disrupted area (marked by arrows) at the intersections of two $\{111\}$ twin traces is clearly visible. This area is circular and about 1.5 nm in diameter. EDX mappings of Al (blue) and Sr (red) are shown in Fig. 6(b). A high intensity of Al has been observed in this area but

only a slightly increased intensity of Sr compared to the surrounding area. This confirms concentration profiles of additional Al-rich regions obtained using APT (see Fig. 4(d)).

The high twin density in Sr-modified eutectic Si fibres observed in the present study is correlated with the presence of Sr–Al–Si co-segregations. Such rod-like Sr–Al–Si co-segregations, stated as type I in Ref. 10, promote "impurity induced twinning". Furthermore, detailed APT and HRTEM analyses in the present paper demonstrated that additional Al-rich regions with spherical morphology are also located at the intersections of twins (see Fig. 6). Since such Al-rich regions are obtained at the same crystallographic features as Sr–Al–Si co-segregations (type I), it is concluded that both of them are responsible for the formation of twins in eutectic Si fibres. However, analysing the plate-like Si in unmodified Al–Si alloys by means of high-resolution methods could help to unambiguously clarify whether such spherical Al-rich regions form even without addition of Sr.

4. Summary

Co-segregations in the Sr-modified eutectic Si phase of Al– 10 wt.% Si alloy were investigated using the complementary high-resolution methods APT and TEM. Two kinds of segregated regions were identified at the intersections of Si twin traces. They differ in composition, size and 3D morphology. Whereas Sr-Al-Si rod-like co-segregations contain about 2.7 at.% Sr, 6.2–11 at.% Al and 86.4–91 at.% Si, additional Al-rich regions contain ≤ 0.5 at.% Sr, 35–65 at.% Al and 65–35 at.% Si. The size of Sr-Al-Si rod-like co-segregations ranges from 1–3 nm in diameter, whereas the size of additional Al-rich regions with spherical morphology ranges from 2–6 nm in diameter. It was found that both kinds of segregated regions are responsible for the formation of a high twin density in the eutectic Si phase.

Acknowledgements

The authors gratefully thank the DFG for financial support via grants Wa 1378/18, Wa 1378/20 and Ba 1170/19. The TEM study was partly carried out on the "Nanotechnology Network Japan" program sponsored by MEXT of the Japanese Government.

References

- [1] Pacz A, Alloy. U.S. Patent No. 1387900;1921.
- [2] M. Makhlof, H. Guthy, The aluminium–silicon eutectic reaction: mechanism and crystallography, *J. Light Met.* 1 (2001) 199-218.
- [3] J.E. Gruzleski, The Art and Science of Modification: 25 Years of Progress, *AFS Trans.* 100 (1992) 673-683.
- [4] S. Hegde, K.N. Prabhu, Modification of eutectic silicon in Al–Si alloys, *J. Mater. Sci.* 43 (2008) 3009-3027.
- [5] D.R. Hamilton, R.G. Seidensticker, Propagation mechanism of germanium dendrites, *J. Appl. Phys.* 31 (1960) 1165-1168
- [6] M.G. Day, A. Hellawell, The microstructure and crystallography of aluminium–silicon eutectic alloys, *Proc. Roy. Soc., A* 305 (1968) 473–491.
- [7] K. F. Kobayashi, L. M. Hogan, The crystal growth of silicon in Al-Si alloys, *J. Mater. Sci.* 20, (1985) 1961-1975.
- [8] S.Z. Lu, A. Hellawell, The mechanism of silicon modification in aluminum–silicon alloys: impurity induced twinning, *Metall. Mater. Trans. A* 18 (1987) 1721–1733.
- [9] K. Nogita, H. Yasuda, K. Yoshida, K. Uesugi, A. Takeuchi, Y. Suzuki, A.K. Dahle, Determination of strontium segregation in modified hypoeutectic Al–Si alloy by micro X-ray fluorescence analysis, *Scripta Mater.* 55 (2006) 787–790.
- [10] M. Timpel, N. Wanderka, R. Schlesiger, T. Yamamoto, N. Lazarev, D. Isheim, G. Schmitz, S. Matsumura, J. Banhart, The role of strontium in modifying aluminium–silicon alloys, *Acta Mater.*, 60 (2012) 3920-3928.
- [11] K. Thompson, D. Lawrence, D. J. Larson, J. D. Olson, T. F. Kelly, B. Gorman, In situ site-specific specimen preparation for atom probe tomography, *Ultramicroscopy* 107 (2007) 131-139.
- [12] P. P. Choi, T. Al-Kassab, Y. S. Kwon, J. S. Kim, R. Kirchheim, Application of focused ion beam to atom probe tomography specimen preparation from mechanically alloyed powders, *Microsc. Microanal.* 13 (2007) 347-353.
- [13] R. Schlesiger, C. Oberdorfer, R. Würz, G. Greiwe, P. Stender, M. Artmeier, P. Pelka, F. Spaleck, G. Schmitz, Design of a laser-assisted tomographic atom probe at Münster University, *Rev. Sci. Instrum.* 81 (2010) 043703.
- [14] F. Lasagni, A. Lasagni, E. Marks, C. Holzapfel, F. Mücklich, H.P. Degischer, Three-dimensional characterization of 'as-cast' and solution-treated AlSi12(Sr) alloys by high resolution FIB tomography, *Acta Mater.* 55 (2007) 3875–3882.
- [15] M. Timpel, N. Wanderka, B.S. Murty, J. Banhart, Three-dimensional visualization of the microstructure development of Sr-modified Al–15Si casting alloy using FIB-EsB tomography, *Acta Mater.* 58 (2010) 6600-6608.
- [16] M. Timpel, N. Wanderka, R. Grothausmann, J. Banhart, Influence of Sr on the formation of Fe-rich phases in Al–10wt% Si casting alloys, *Acta Mater.*, submitted (2012).
- [17] M. Gilbert, F. Vurpillot, A. Vella, H. Bernas, B. Deconihout, Some aspects of the silicon behaviour under femtosecond pulsed laser field evaporation, *Ultramicroscopy*, 107 (2007) 767-772.

- [18] O.C. Hellman, J.A. Vandenbroucke, J. Rüsing, D. Isheim, D.N. Seidman, Analysis of three-dimensional atom probe data by the proximity histogram, *Microsc. Microanal.* 6 (2000) 437-444.
- [19] M. Timpel, N. Wanderka, G.S. V. Kumar, J. Banhart, Microstructural investigation of Sr-modified Al–15wt%Si alloys in the range from micrometer to atomic scale, *Ultramicroscopy*, 111 (2011) 695–700.
- [20] M. Shamsuzzoha, L.M. Hogan, Crystal morphology of unmodified aluminum-silicon eutectic microstructures, *J. Cryst. Growth* 76 (1986) 429–439.
- [21] M. Shamsuzzoha, L.M. Hogan, The crystal morphology of fibrous silicon in strontium modified Al–Si eutectic, *Phil. Mag. A* 54 (1986) 459–477.
- [22] S.C. Flood, J.D. Hunt, Modification of Al–Si eutectic alloys with Na, *Met. Sci.* 15 (1981) 287-294.

Table 1. Chemical composition of Sr-modified Al– 10 wt.% Si alloy measured by optical emission spectrometry. The amounts of Al, Si and Fe are given in wt.%. The amounts of all other elements are in ppm.

Al	Si	Fe	Cu	Mn	Mg	Cr	Ti	Ni	Ga	V	B	P	Mo	Ca	Sr
wt. %			ppm												
89.1	10.0	0.1	10	20	10	11	60	38	42	102	6	4	3	1	200

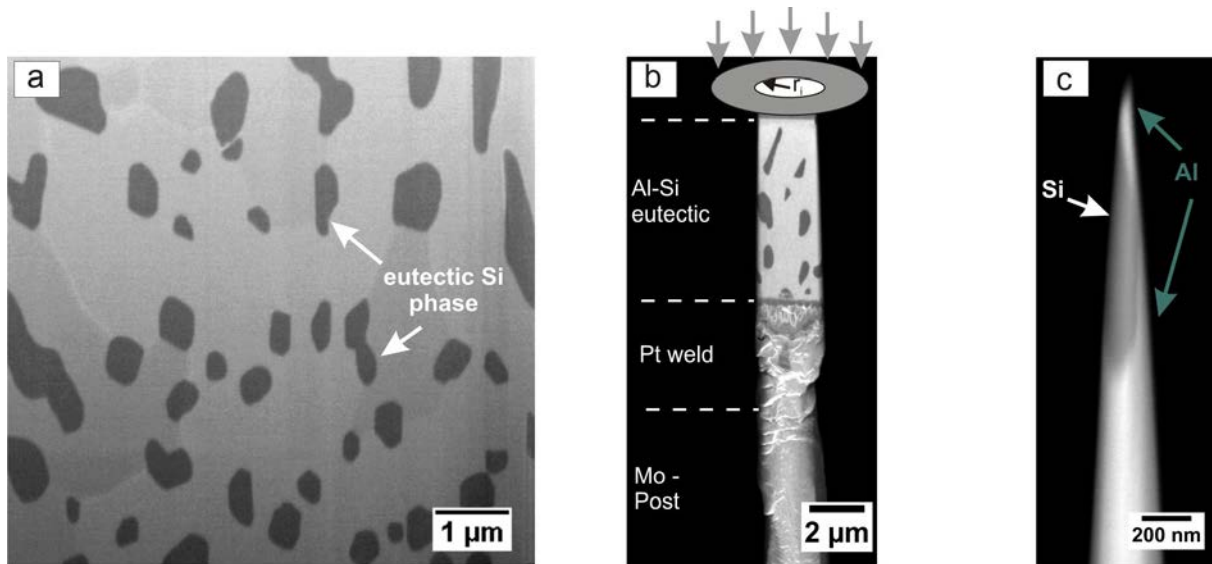


Fig. 1. (a) Eutectic microstructure of the Sr-modified Al– 10 wt.% Si alloy imaged by SEM. (b,c) SEM images of atom probe specimen preparation steps: (b) Al-Si eutectic mounted onto electrolytically etched post via FIB *liftout* technique, (c) specimen after final FIB sharpening with a final tip radius of ~ 30 nm. The apex of the tip contains a Al/Si eutectic interface.

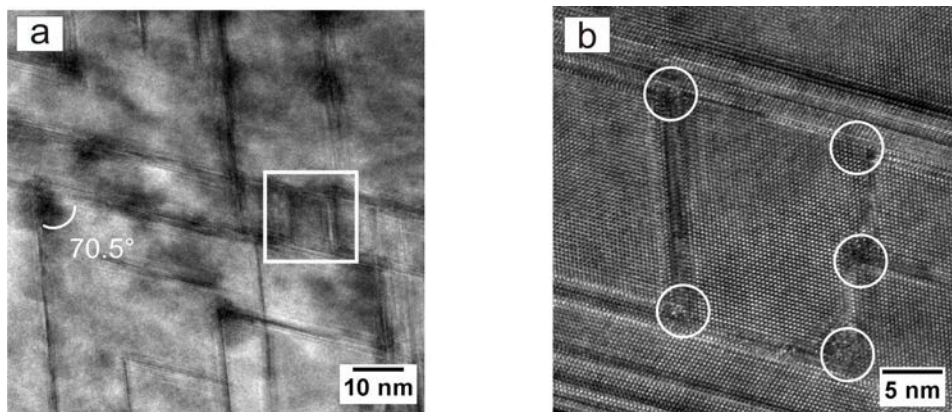


Fig. 2. Microstructure showing region of high twin density within eutectic Si fibre of the Sr-modified Al– 10 wt.% Si alloy: a) BF STEM of $\{111\}_{\text{Si}}$ planes imaged with $\langle 110 \rangle$ orientation. Many areas of dark contrast are mainly located at the intersection of Si twins. (b) HRTEM micrograph of an enlarged view of the area marked by the rectangle in (a). Si crystal lattice with disrupted areas (marked by circles) at the intersection of two twins are clearly visible.

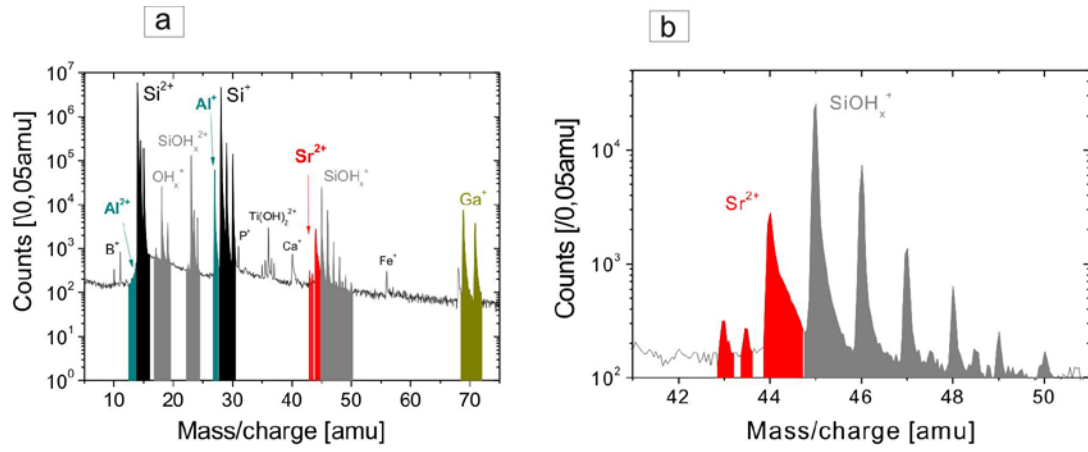


Fig. 3. Atom probe mass spectrum of a eutectic Si fibre in the Sr-modified Al– 10 wt.% Si alloy. (a) Mass spectrum range of 5–75 amu and (b) mass spectrum range of 40–52 amu.

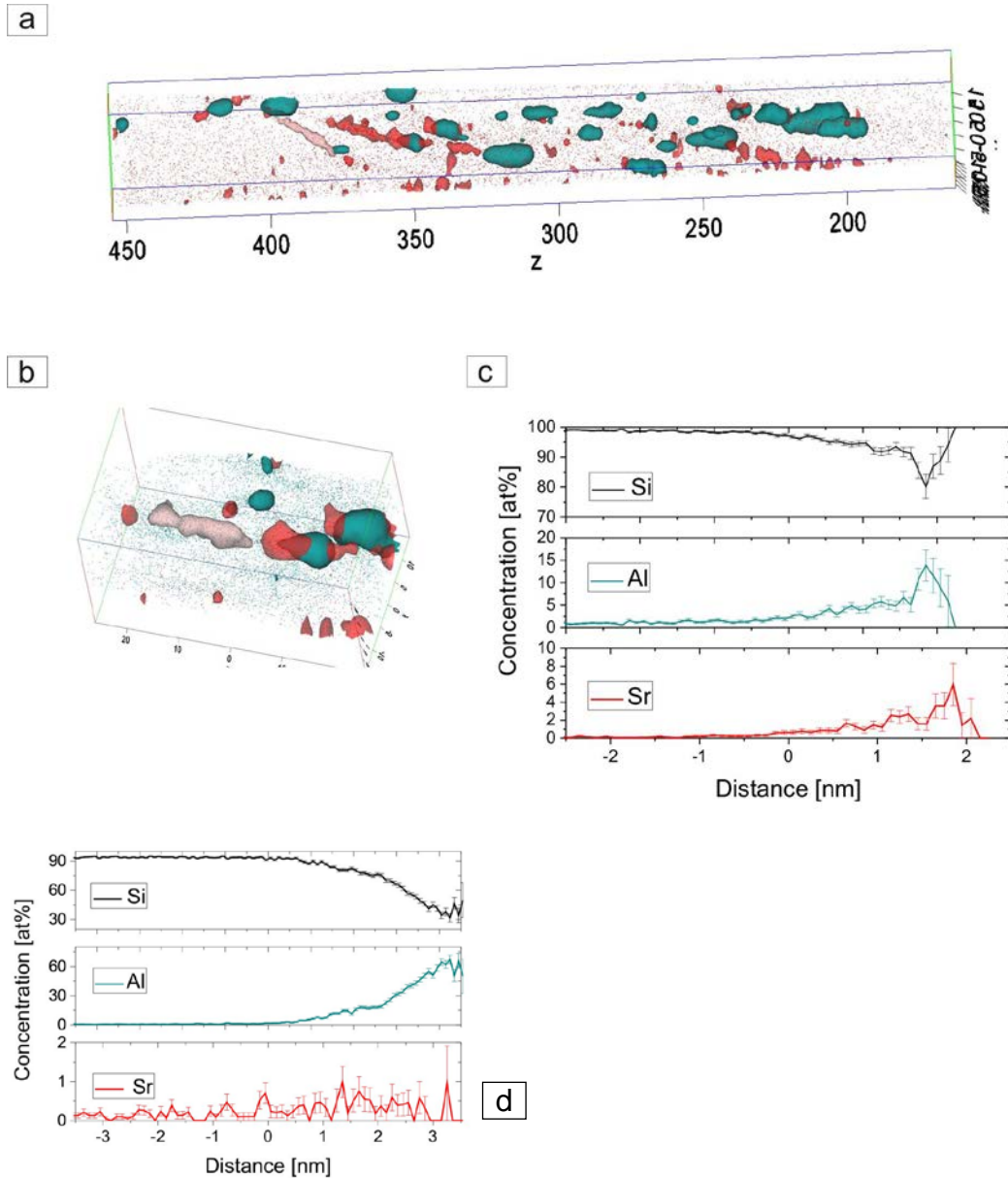


Fig. 4. Atom probe tomography of a eutectic Si fibre in the Sr-modified Al–10 wt.% Si alloy: (a) 3D reconstruction of Sr atoms (red dots) and regions captured by iso-concentration surfaces with Sr concentrations > 0.6 at.% (red) and Al concentrations > 5 at.% (blue) in an analysed volume of $39 \times 38 \times 290 \text{ nm}^3$. (b) Sr–Al–Si co-segregations and a few spherical Al-rich regions within an analysed volume of $30 \times 30 \times 50 \text{ nm}^3$. (c) Proximity histogram showing Sr, Al and Si concentrations as a function of distance to the defined Si/Sr–Al–Si co-segregation interfaces (0.6 at.% Sr) given in (b). (d) Proximity histogram showing Sr, Al and Si concentrations as a function of distance to the defined Si/Al-rich region interfaces (5 at.% Al) given in (b).

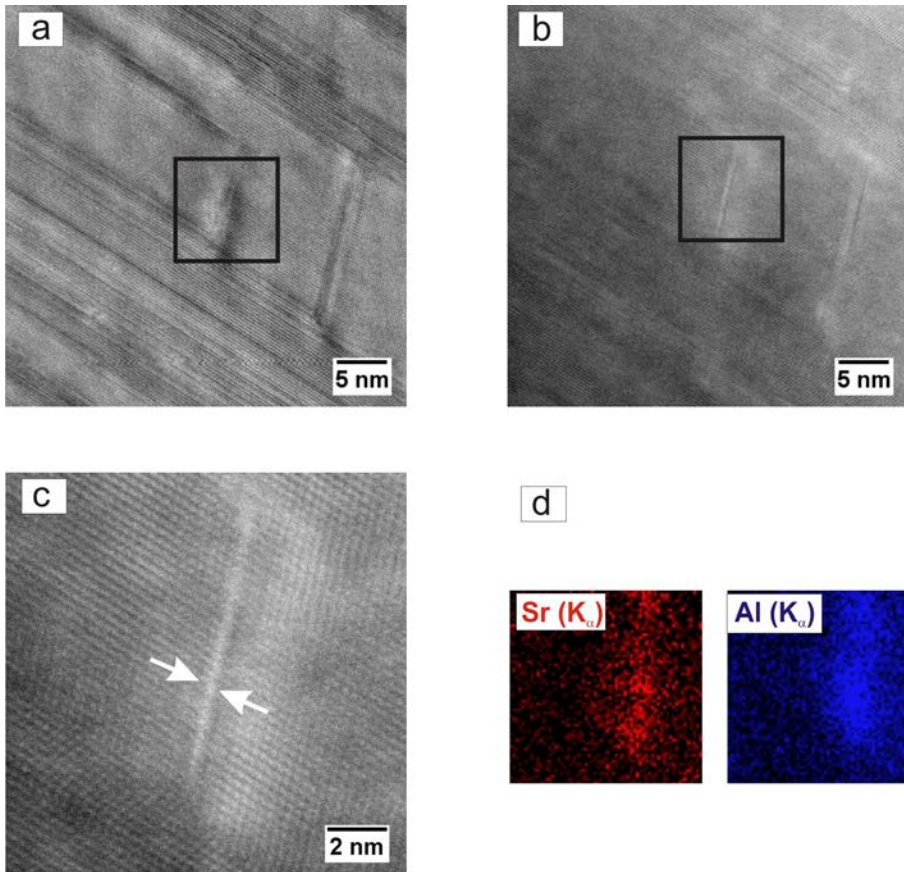


Fig. 5. Microstructure of one and the same area within a eutectic Si fibre in the Sr-modified Al– 10 wt.% Si alloy obtained using (a) BF STEM; (b) HAADF STEM; (c) enlarged view of the area marked by the rectangle in (b); (d) EDX mapping of Al (blue) and Sr (red) within the area shown in (c).

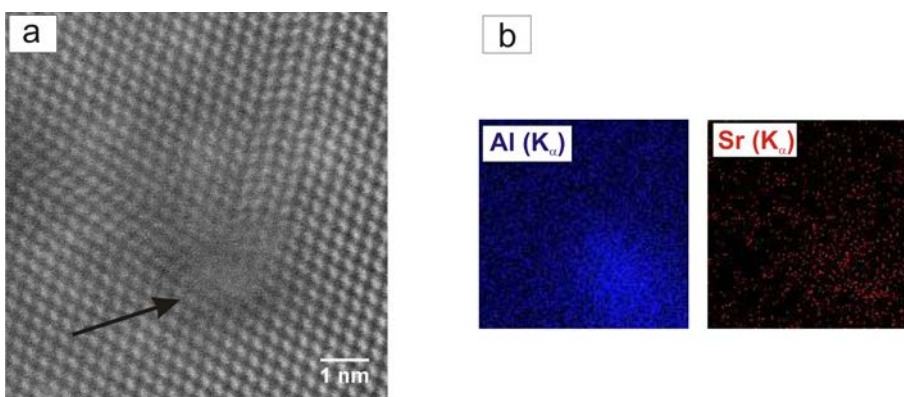


Fig. 6. Microstructure showing one and the same area within a eutectic Si fibre in the Sr-modified Al– 10 wt.% Si alloy obtained using (a) BF STEM of $\{111\}_{\text{Si}}$ planes imaged with $\langle 110 \rangle$ orientation. Lattice with disrupted area (marked by arrows) at the intersection of two Si twins is visible. (b) EDX mapping of Al (blue) and Sr (red) of area shown in (a).